



New Journal of Physics

The open-access journal for physics

Multi-band spectroscopy of inhomogeneous Mott-insulator states of ultracold bosons

D Clément¹, N Fabbri, L Fallani, C Fort and M Inguscio

LENS, Dipartimento di Fisica, Università di Firenze and INFN-CNR,
via Nello Carrara 1, I-50019 Sesto Fiorentino (FI), Italy
E-mail: clement@lens.unifi.it

New Journal of Physics **11** (2009) 103030 (18pp)

Received 11 June 2009

Published 21 October 2009

Online at <http://www.njp.org/>

doi:10.1088/1367-2630/11/10/103030

Abstract. In this work, we use inelastic scattering of light to study the response of inhomogeneous Mott-insulator gases to external excitations. The experimental setup and procedure to probe the atomic Mott states are presented in detail. We discuss the link between the energy absorbed by the gases and accessible experimental parameters as well as the linearity of the response to the scattering of light. We investigate the excitations of the system in multiple energy bands and a band-mapping technique allows us to identify band and momentum of the excited atoms. In addition, the momentum distribution in the Mott states that is spread over the entire first Brillouin zone enables us to reconstruct the dispersion relation in the high energy bands using a single Bragg excitation with a fixed momentum transfer.

¹ Author to whom any correspondence should be addressed.

Contents

1. Introduction	2
2. Inelastic light scattering from correlated gases in optical lattices	3
2.1. Inelastic light scattering as a probe of excitations	3
2.2. Two-photon Bragg transitions	4
2.3. Calibration of the momentum transfer	5
3. Amount of excitation and linear response regime	6
3.1. Energy transfer by the Bragg beams to a gas loaded in optical lattices	6
3.2. Amount of excitation \mathcal{A}	8
3.3. Linear response regime	9
4. Excitations in inhomogeneous Mott states towards different energy bands	10
4.1. Multi-band spectrum of a MI state	11
4.2. Measurement of the momentum of the excited atoms by the Bragg beams	13
4.3. High-energy bands; towards novel information about the Mott state	14
5. Conclusion	16
Acknowledgments	16
References	17

1. Introduction

Many-body quantum systems where strong correlations between particles play a central role are among the most intriguing physical systems since no simple picture captures their behavior. Examples of this kind can be found in correlated electronic systems such as high- T_c superconductors [1], quantum liquids such as liquid helium [2] or interacting one-dimensional (1D) systems [3] such as carbon nanotubes [4], quantum wires [5] and organic conductors [6]. A large amount of research work has been devoted to the study of such systems within different fields of physics, yet many questions have still to be addressed. In this prospect, new experimental possibilities have been opened by the realization of degenerate quantum gases and the recent development of techniques to manipulate them in optical lattices. Indeed, in recent years ultracold atomic gases have been loaded in optical lattices to create strongly correlated quantum phases in a highly controllable manner.

Among these experiments, different atomic insulating phases have been realized demonstrating the versatility of gaseous systems. These include bosonic Mott insulators (MIs) in 1D, 2D and 3D systems [7]–[9], disordered bosonic insulating phases [10] as well as fermionic MIs [11, 12]. The characterization of these insulating quantum phases has enlightened many of their properties. Experiments have demonstrated the presence of a gap in the spectrum of MIs [7, 9] and its vanishing in a disordered insulating phase [10]. A noise correlation analysis of time-of-flight pictures has shown the spatial order of the atomic distribution [13] and its controlled modification when changing the lattice potential [14]. Studies of the suppression of compressibility has been performed in fermionic [11, 12] and bosonic [15] MIs. In addition to these properties expected in homogeneous insulating phases, the presence of a trap enriches the experimental situation while creating alternate regions of Mott with different filling factors and superfluid (SF) states [16, 17]. This shell structure has been identified in experiments and clearly related to the trapping potential [18, 19]. Recently, inelastic light scattering has been

used to measure the excitation spectrum of inhomogeneous MI states [20]. This spectroscopic measurement performed at nonzero momentum transfer and in the linear response regime gives a direct access to the dynamical structure factor S of those complex phases [21]–[26].

In this paper, we report the measurement of the excitation spectrum of 1D bosonic MI states over several energy bands. The band structure is induced by the presence of the optical lattice, which drives the system into a MI state. A particular attention is paid to the details of the spectroscopic technique. We discuss the measurement of the energy absorbed by the atomic system when excitations are created as well as the linearity of its response. This paper also extends our previous work [20], the scope of which was centered on the study of excitations lying in the lowest energy band. We present experimental results for the spectra in the higher energy bands showing novel experimental signatures related to the one-particle spectral function of the Mott state. A band-mapping technique is used to identify the momentum of the excited atoms contributing to the different parts of the spectra in the inhomogeneous Mott state.

The paper is organized as in the following. In section 2, we describe the principles and the experimental implementation of inelastic light scattering (Bragg spectroscopy) as a probe of excitations of ultracold atoms in optical lattices. In section 3, we present the experimental sequence allowing to extract information about the amount of excitation created by the Bragg beams. We discuss the choice of the experimental parameters in order to work in the linear regime, in particular for the response of MI states. Section 4 is devoted to the multi-band spectra of the inhomogeneous MI states and to the band-mapping technique. The latter allows us to directly reconstruct the dispersion relation in the high-energy bands induced by the optical lattice. Finally, we discuss the relation of the high-energy band spectra with the measurement of the one-particle spectral function of the atomic Mott state.

2. Inelastic light scattering from correlated gases in optical lattices

2.1. Inelastic light scattering as a probe of excitations

The result of weak inelastic scattering of waves or particles by many-body systems may be described within the Born approximation and expressed in terms of the dynamic structure factor S [27]. The dynamic structure factor is the Fourier transform of the density–density correlation function and it carries information on the excitation spectrum of the system, independently from the external probe. The knowledge of the dynamic structure factor S obtained from inelastic scattering processes has proved to be central in describing many-body systems, from the electrons in solids [28] to SF helium [2].

Inelastic light scattering has been applied to gaseous Bose–Einstein condensates (BECs) to measure the dynamic structure factor [29]–[31]. This scattering technique, referred to as Bragg spectroscopy, consists in a two-photon transition between two different momentum states of the same internal ground state [29]. The dispersion relation of interacting BECs in the mean-field regime [32]–[34], the presence of phase fluctuations in elongated BECs [35] as well as signatures of vortices [36] have been investigated using this technique. Bragg spectroscopy is also used as a tool to coherently manipulate atomic clouds for interferometric schemes ([37] and references therein) or for thermodynamics studies [38, 39]. More recently, it has succeeded in providing novel information about strongly interacting 3D Bose [40] and Fermi [41] gases close to Feshbach resonances as well as correlated 1D Bose gases across the transition from the SF to the MI state [20].

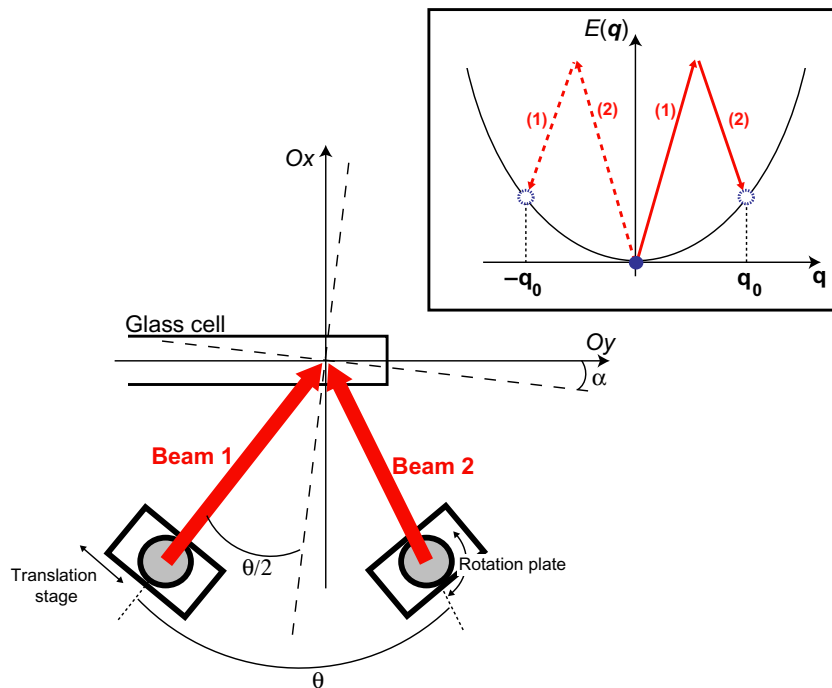


Figure 1. Experimental setup: two laser beams (red), detuned with respect to each other by a controllable frequency ν , are shone onto the atoms in the glass cell in order to induce a two-photon transition. The direction of each beam can be changed thanks to a rotation plate and a translation stage that allow a precise control of the angle θ . The axes (Ox, Oy) coincide with the axes of the lattice beam (see text below). Inset: parabolic energy spectrum of free particles. Depending on the sign of the relative detuning ν between the Bragg beams atoms absorb photons from beam 1 and emit in beam 2 (for $\nu > 0$, solid lines) or absorb from beam 2 and emit in beam 1 (for $\nu < 0$, dashed lines), changing the direction of the momentum transfer $\hbar\mathbf{q}_0$.

2.2. Two-photon Bragg transitions

The Bragg spectroscopy technique consists in shining the atoms for a finite time t_B with two laser beams detuned by δ from an atomic transition. During the Bragg pulse, atoms absorb photons from one beam and are stimulated to emit photons in the second beam. The resonance condition for the two-photon transition consists of conserving energy and momentum. An atom with an initial momentum \mathbf{p}_i ends up in the same internal state with a final momentum $\mathbf{p}_f = \mathbf{p}_i + \hbar\mathbf{q}_0$, where $\hbar\mathbf{q}_0$ is the momentum transfer given by the two-photon process. The energy difference between the initial and final atomic states is also given by the Bragg beams, which are detuned from each other by a frequency $\nu = \nu_1 - \nu_2$ where ν_1 and ν_2 are the frequencies of the two beams (see figure 1). In practice, by tuning the frequency difference ν , one can match the resonance energy for the two-photon transition process to occur at a given momentum transfer $\hbar\mathbf{q}_0$. In other words, this corresponds to the condition for which the atomic wave function is efficiently diffracted on the moving optical lattice created by the Bragg beams. We note V_B the amplitude of the lattice induced by the Bragg beams and $\Omega_B/2\pi = V_B/2h$ the associated Rabi frequency.

The modulus of the momentum transfer $\hbar\mathbf{q}_0$ given to the atoms is set by the wavelength λ_B of the Bragg beams and the angle θ between them, namely $q_0 = 4\pi/\lambda_B \sin(\theta/2)$ (see figure 1). Note that the direction of \mathbf{q}_0 is perpendicular to the bisector between the two beams. The detuning ν between the two Bragg beams controls not only the energy $h\nu$ transferred to the atoms but also the sign of the momentum transfer. For a two-photon transition towards an excited state with higher kinetic energy, atoms absorb a photon from the beam with the higher energy photons and are stimulated to emit a photon in the beam with the lower energy photons. Therefore, with our convention, when the detuning $\nu = \nu_1 - \nu_2$ is positive atoms absorb photons from beam 1, emit into beam 2 and the momentum transfer is $+\hbar\mathbf{q}_0$ (see inset in figure 1). When the detuning ν is negative atoms absorb from beam 2, emit into beam 1 and the momentum transfer is opposite, i.e. $-\hbar\mathbf{q}_0$.

In our experimental setup, a laser beam coming out from a laser diode at wavelength $\lambda_B = 780$ nm, detuned by $\delta \simeq 300$ GHz from the D2 transition of ^{87}Rb , is separated into two beams, each passing through an acousto-optic modulator (AOM). The two AOMs are locked in phase and allow to control the relative detuning ν ($\nu = \nu_1 - \nu_2 \ll \delta$) between the two Bragg beams. After passing through the AOMs, each beam is injected into a polarization-maintaining fiber. The out-coupler of each fiber is fixed onto a post-holder mounted on a rotation plate and a translation stage close to the cell in which the atoms are manipulated. This setup allows an independent control of the angle of each of the Bragg beams with respect to the y -axis (see figure 1). In particular, the angle θ between the two Bragg beams can be tuned from 30° to 60° , this range being determined by the limited optical access to the glass cell. While λ_B is precisely known in the experiment, the angle θ cannot be measured geometrically with high precision. We use the atoms as a sensor to precisely calibrate \mathbf{q}_0 . To this purpose we measure the momentum transferred to a 3D BEC (in the absence of any optical lattice) in two different ways.

2.3. Calibration of the momentum transfer

In the first calibration measurement, we measure the resonant frequency of the Bragg spectrum for the 3D BEC. The resonance frequency depends on the momentum transfer $\hbar\mathbf{q}_0$, on the strength of atom–atom interactions through the dispersion relation and on the initial velocity of the BEC center-of-mass. The dispersion relation $E(\mathbf{q})$ of a trapped 3D BEC in the mean-field regime can be written as

$$E(\mathbf{q}) = \hbar \sqrt{c_{\text{LDA}}^2(\mathbf{q})\mathbf{q}^2 + \left(\frac{\hbar\mathbf{q}^2}{2m}\right)^2}, \quad (1)$$

where $c_{\text{LDA}}(\mathbf{q})$ corresponds to an effective sound velocity within a local density approximation and is related to the mean-field interaction term [42]. The two-photon transition induced by the Bragg pulse couples the initial state of the 3D BEC with momentum $\mathbf{p}_i = \hbar\mathbf{q}_i$ to an excited state with momentum $\mathbf{p}_f = \hbar(\mathbf{q}_i + \mathbf{q}_0)$. Thus the resonance energy of this process is $E(\mathbf{q}_i + \mathbf{q}_0) - E(\mathbf{q}_i)$. In the absence of interactions, this energy reduces to the usual quadratic dependence of a single-particle spectrum, i.e. $\hbar^2(\mathbf{q}_i + \mathbf{q}_0)^2/2m - \hbar^2\mathbf{q}_i^2/2m$. In order to reduce the effect on evaluating \mathbf{q}_0 coming from interactions, we perform Bragg spectroscopy on dilute 3D BECs after a time-of-flight. When the magnetic trap is switched off the BEC acquires a spurious nonzero momentum $\hbar\mathbf{q}_i$ and two unknown parameters have to be determined, namely \mathbf{q}_0 and \mathbf{q}_i . We measure the spectra at positive ($\hbar\mathbf{q}_0$) and negative ($-\hbar\mathbf{q}_0$) momentum transfer.

The two resonance frequencies $E(\mathbf{q}_i + \mathbf{q}_0) - E(\mathbf{q}_i)$ and $E(\mathbf{q}_i - \mathbf{q}_0) - E(\mathbf{q}_i)$ allow us to precisely determine q_0 in the experiment. We obtain $q_0 = 0.97(3)k_L$ where $k_L = 2\pi/\lambda_L$ is the wave vector of the lattice beams (see text below) at the wavelength $\lambda_L = 830$ nm.

In the experiment, the bisector of the two Bragg beams is not exactly perpendicular to the y -axis and the momentum transfer along the y -axis is the projection $\hbar q_{0,y} = 4\hbar\pi \cos(\alpha)/\lambda_B \sin(\theta/2)$ where α is the angle as defined on figure 1. Note that the axes on figure 1 are defined as the axes of the lattice beams (see below). To measure the angle α we diffract the atoms in the Raman–Nath regime [43] with very short light pulses (of typical duration $3 \mu\text{s}$). In this diffraction regime, many clouds of diffracted atoms are observed allowing a good estimate of the axis of the momentum transferred to the atoms. We use such a procedure for both the lattice beams and the Bragg beams separately, measuring the angle $\alpha = 9.5(1)^\circ$ (see figure 1). As a consequence the projection of the momentum transfer along the y -axis is $\hbar q_{0,y} = 0.96(3)\hbar k_L$.

In a second set of calibration measurements, we use the diffracted atoms of the 3D BEC by the moving lattice created with the Bragg beams. By letting the atoms fall under gravity after the Bragg pulse for a long enough time-of-flight ($t_{\text{TOF}} = 10\text{--}30$ ms), the diffracted atoms separate from the atoms which have not undergone the two-photon transition. The distance between the two clouds is $\hbar q_{0,y} t_{\text{TOF}}/m$ in the yOz plane where absorption images are taken, m being the atomic mass. By fitting the distance between the diffracted and non-diffracted atomic clouds as a function of t_{TOF} , we measure $q_{0,y} = 0.97(4)k_L$ in good agreement with the previous measurement.

3. Amount of excitation and linear response regime

3.1. Energy transfer by the Bragg beams to a gas loaded in optical lattices

3.1.1. Experimental setup and time sequence. We use the Bragg spectroscopic scheme described in section 2 to probe the response of correlated 1D Bose gases in the linear response regime [20]. Correlated Bose phases are created by loading a 3D BEC of ^{87}Rb atoms in a 3D optical lattice as described in previous papers [10, 20]. In brief, a 3D BEC of $N \sim 1.5 \times 10^5$ atoms is produced in a magnetic trap whose frequencies are $\omega_x = \omega_z = 2\pi \times 90$ Hz and $\omega_y = 2\pi \times 8.9$ Hz. Then it is adiabatically loaded in a 3D optical lattice created with three pairs of counter-propagating laser beams at the wavelength $\lambda_L = 830$ nm. The amplitudes V_i of the optical lattice along each axis $i = x, y, z$ are expressed in units of the recoil energy $E_R = \hbar^2/2m\lambda_L^2$, $V_i = s_i E_R$. The optical lattices are ramped up to their final values s_i with an exponential ramp of duration 140 ms and time constant 30 ms.

In all the experiments described in this paper, a 2D optical lattice in the plane xOz with amplitudes $s_x = s_z = s_\perp = 35$ is used to create an array of 1D tubes of atoms. At this amplitude s_\perp and in the absence of the longitudinal lattice ($s_y = 0$), we measure the ratio of the frequencies of the quadrupole mode ν_Q to the dipole mode ν_D to check that the 1D gases are Bose condensed. For holding times in the 2D lattice (at $s_\perp = 35$) up to 50 ms, this ratio is close to the value $\sqrt{3}$ corresponding to the expected value for 1D Bose-condensed gases close to the mean-field regime [44, 45]. For longer holding times, the ratio increases up to the value 2 expected for a thermal 1D Bose gas. All the experiments are performed with a typical holding time at the amplitude $s_\perp = 35$ equal to 10 ms ensuring the 1D gases are Bose condensed in the absence of the longitudinal lattice ($s_y = 0$).

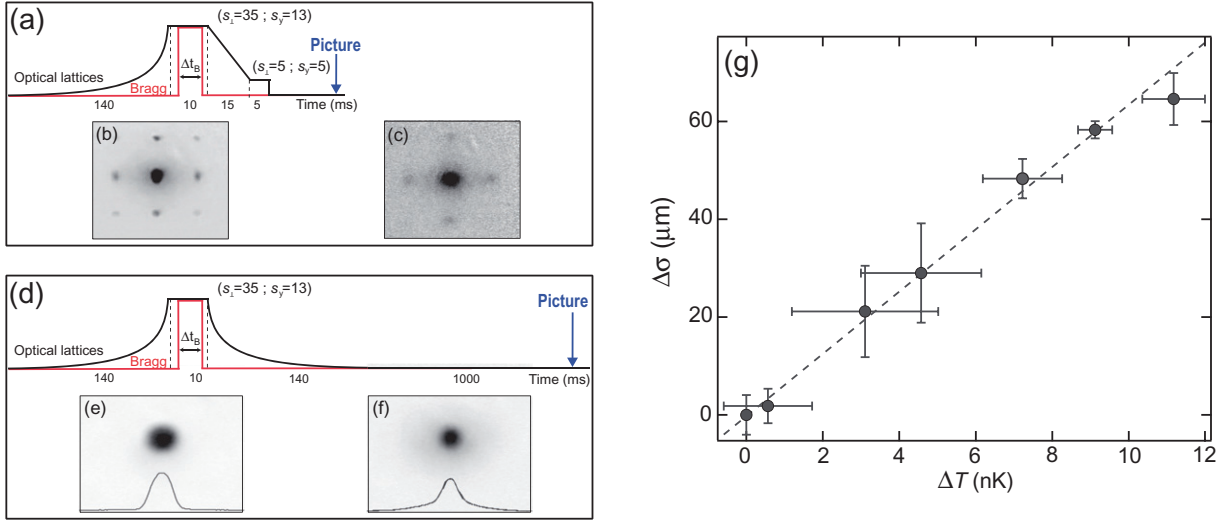


Figure 2. (a) Experimental sequence to measure the increase $\Delta\sigma$ of the width of the central peak of the interference pattern after a Bragg pulse. Picture (b) (resp (c)) corresponds to an absorption image taken after a non-resonant (resp resonant) Bragg pulse. (d) Experimental sequence to measure the increase of temperature ΔT after a Bragg pulse and a thermalization time of 1 s. Picture (e) (resp (f)) corresponds to an absorption image taken after a non-resonant (resp resonant) Bragg pulse. (g) $\Delta\sigma$ as a function of the increase of temperature ΔT . The points correspond to different power of the Bragg beams with a fixed pulse length of 3 ms.

The amplitude s_y of the optical lattice is changed to tune the 1D gases from a correlated SF state ($s_y = 0$) to inhomogeneous MI states ($s_y > 6$). For large amplitudes s_y the dynamics of 1D gases (when restricted to the lowest energy band of the optical lattice along Oy) can be described by the Bose–Hubbard Hamiltonian [16],

$$H = -J \sum_{\langle i,j \rangle} (a_i^\dagger a_j + \text{h.c.}) + \frac{U}{2} \sum_i n_i (n_i - 1) + \sum_i \epsilon_i n_i. \quad (2)$$

Here a_i^\dagger , a_i are the creation and annihilation operator of one boson at site i and $n_i = a_i^\dagger a_i$ is the particle number operator. The on-site interaction energy is given by U and the next-neighbor hopping amplitude by J . ϵ_i is the slowly varying energy offset experienced by an atom on site i due to the presence of the harmonic confining potential.

Once the amplitude of the 3D optical lattice has reached its final values ($s_\perp = 35$, s_y) the Bragg pulse is shone onto the system for a time t_B (see figure 2(a)). In order to detect the amount of excitation induced by the Bragg beams in the correlated gaseous systems, we follow a procedure similar to that used in [7] and described in [20] that consists in measuring a quantity related to the increase of energy in the gas.

3.1.2. Measurement of the energy transfer. After shining the Bragg pulse onto the atoms the amplitudes of the 3D lattice are ramped down linearly to $s_\perp = s_y = 5$ in 15 ms where we let the system rethermalize for 5 ms (see figure 2(a)). Then the magnetic trap and the 3D lattice are

switched off abruptly and an absorption image of the atomic distribution in the yOz plane is taken after a typical time-of-flight $t_{\text{TOF}} \simeq 22$ ms. Expanding from a phase coherent state in a 3D optical lattice ($s_{\perp} = s_y = 5$), the atomic distribution exhibits an interference pattern which is the analogous of the diffraction pattern of light from a grating (see figure 2(b) and [46]). From this interference pattern we extract the rms widths σ_y and σ_z of the central peak, the increases of which are related to that of the energy of the system. Indeed, when the Bragg excitation is tuned out of resonance both widths σ_y and σ_z are equal to the widths measured in the absence of the Bragg pulse while on resonance they increase (see figure 2(c)). Moreover, we find that σ_y and σ_z have the same dependence with the detuning ν between the Bragg beams as expected from an efficient rethermalization process in each spatial direction when the lattices are ramped down. In the following, we will consider an average width σ defined as $\sigma = \sqrt{\sigma_y \sigma_z}$.

To be more quantitative on the relation between the increase of σ , denoted $\Delta\sigma$, and the energy absorbed by the gas, we make a comparison of $\Delta\sigma$ after a resonant Bragg excitation with a measurement of the temperature increase ΔT realized in the same experimental conditions (in particular, for an identical Bragg excitation). The temperature is obtained by ramping down adiabatically the optical lattices with an exponential ramp after the Bragg pulse, letting the system thermalize in the magnetic trap for 1 s and measuring the condensate fraction of the 3D atomic cloud (see figure 2(d)). The comparison is performed by setting the detuning ν on the resonance towards the second band in the case of an inhomogeneous MI state with $s_y = 13$ (see section 4). By changing the power in the Bragg beams, $\Delta\sigma$ is tuned over a range typical of that used in experiments. The results are presented in figure 2 where ΔT is extracted from the decrease of the condensate fraction. This measurement confirms that $\Delta\sigma$ is proportional to the energy absorbed by the atomic system, i.e. to the number of excitations created.

One may wonder whether the spectra could be obtained measuring the condensate fraction instead of the width σ . This could be the case when the amplitude of the response of the 1D gases is large as in the SF regime or in the Mott regime for high-energy bands. In contrast, the amplitude of the response of the MI state within the lowest energy band is low as the system exhibits its insulating behavior. In this case, we observe that the measurement of $\Delta\sigma$ is more sensitive than that of the condensate fraction, allowing to detect small excitations.

3.2. Amount of excitation \mathcal{A}

We now describe the quantity we will be referring to as the amount of excitations. This quantity is proportional to the increase $\Delta\sigma$ of the central peak width of the interference pattern obtained after a time-of-flight (see figure 2(b) and text below). It is rescaled as explained in the following.

The width σ of the central peak has a weak dependence on the total atom number N , which is related to the presence of interactions, independently from the Bragg excitation. In the experiment, the total atom number typically fluctuates by 20% from shot-to-shot. In order to remove the small variations (up to 8%) on the measurement of σ coming from fluctuations of N , we calibrate the increase of σ with N by changing the atom number over a wide range 10^5 – 10^6 . This scaling has been used to subtract, for each measurement of σ , the contribution to σ coming from the fluctuations in the atom number. To display the spectrum the width in the absence of Bragg excitation is subtracted in order to plot the increase $\Delta\sigma$. In addition, we rescale $\Delta\sigma$ by the parameters of the Bragg excitation, namely by the factor $(P_B t_B / \delta)^{-1}$ where P_B is the power of the Bragg beams, δ their detuning with respect to the atomic transition and

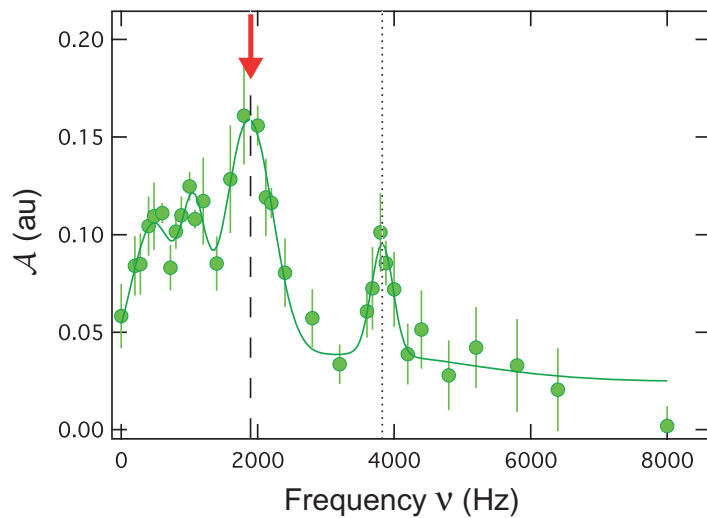


Figure 3. Bragg spectrum of an inhomogeneous MI state with lattice amplitudes $s_{\perp} = 35$ and $s_y = 13$. The dashed (resp dotted) vertical line marks the resonance energy $\Delta_{\text{ph}} \sim U$ (resp $2\Delta_{\text{ph}} \sim 2U$) of the Mott state. The red arrow indicates the detuning ν at which the linearity of the response has been tested. It corresponds to the resonance energy of a particle–hole excitation in the Mott regions.

t_B the duration of the Bragg pulse². This procedure allows us to compare the amplitudes of the response for spectra taken with slightly different parameters of the Bragg beams. The linear dependence of $\Delta\sigma$ with $(P_B t_B / \delta)^{-1}$ holds in the linear response regime, the validity of which we discuss below. In the following, we will refer to the rescaled $\Delta\sigma$, called \mathcal{A} , as to the amount of excitation transferred to the system. The plot of \mathcal{A} as a function of the detuning ν between the two Bragg beams gives the excitation spectrum. In figure 3, we show an example of a spectrum of the inhomogeneous MI state (see text below and [20]).

3.3. Linear response regime

The linearity of the response of the system to the Bragg excitation is studied monitoring how $\Delta\sigma$ varies with the parameters of the Bragg excitation on resonance. In [20], we have identified the particle–hole excitation energy Δ_{ph} of the MI state. Here, we fix the frequency $\nu = \Delta_{\text{ph}} / h$ (i.e. on the resonant peak of the MI state, see red arrow in figure 3) to study the variations of $\Delta\sigma$ as a function of the amplitude V_B of the Bragg lattice and the duration Δt_B of the pulse, with the results plotted in figure 4. In the range of parameters used to monitor the spectra (for example $V_B = 0.5E_R$ and $\Delta t_B = 6$ ms for the spectrum in figure 3 at $s_y = 13$), the increase of $\Delta\sigma$ is linear both with V_B and Δt_B , demonstrating that the energy transferred to the gases by the Bragg pulse increases linearly with both those quantities.

The inset of figure 4(b) compares the variation of $\Delta\sigma$ as a function of the pulse duration Δt_B for two amplitudes V_B , namely $V_B = 0.5E_R$ (dots) and $V_B = 2.0E_R$ (circles) at $\nu = \Delta_{\text{ph}} / h$ for $s_y = 13$. For the larger amplitude $V_B = 2.0E_R$ the response to the Bragg excitation exhibits a

² In [20], we used a slightly different scaling for the amplitude of the response with the parameters of the Bragg in order to normalize the different spectra, namely $(P_B^2 t_B / \delta^2)^{-1}$.

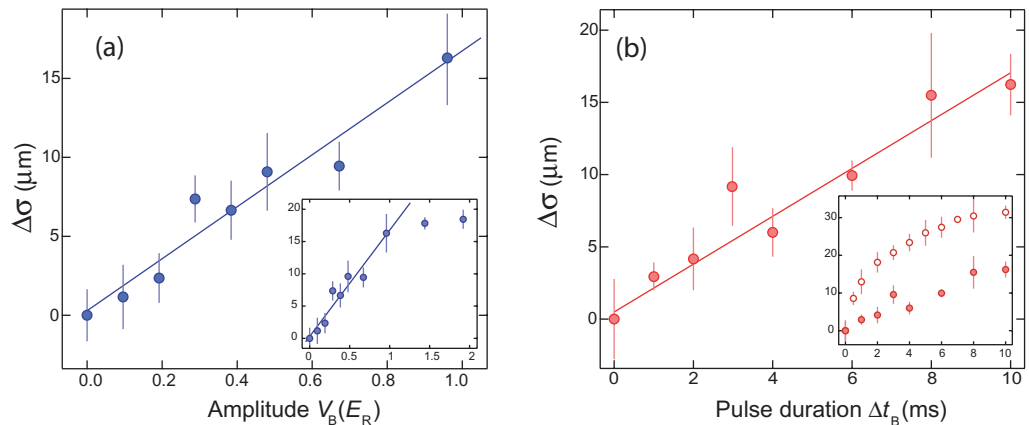


Figure 4. (a) $\Delta\sigma$ as a function of the amplitude V_B of the lattice induced by the Bragg beams, which is proportional to the power P_B . The measurement is performed at a fixed energy transfer $\nu = \Delta_{\text{ph}}/h$ corresponding to the resonance of the particle–hole excitation and for a duration of the Bragg pulse $\Delta t_B = 3$ ms. Inset: same measurement on larger scale of the amplitude V_B showing saturation for $V_B > E_R$. (b) $\Delta\sigma$ as a function of the duration of the Bragg pulse at a given amplitude $V_B = 0.5E_R$. As in (a), the measurement is performed at the energy $\nu = \Delta_{\text{ph}}/h$ of the particle–hole excitation. Inset: comparison of the response for two amplitudes V_B , namely $V_B = 0.5E_R$ (dots) and $V_B = 2.0E_R$ (circles).

saturation and the timescale of the linear regime is shorter. We note that we did not observe Rabi oscillations as in the case of an excitation from the ground state of a 3D BEC in a harmonic trap and a Bogoliubov mode [31]. In the latter case, the excited state is decoupled from the ground state, a situation that might not be true anymore in the Mott state where strong correlations are present. The increase of $\Delta\sigma$ also saturates for large amplitudes V_B as depicted in the inset of figure 4(a).

In addition, we stress that the amplitude V_B of the moving lattice created by the Bragg beams for such parameters is much smaller than the amplitude s_y of the longitudinal lattice: all experiments are performed in a regime where $V_B < 0.05V_y$. This regime is different from the one where the Bragg spectrum has been obtained using the lattice modulation technique. In the latter case, the amplitude of the lattice is typically modulated by 20%–30% due to a momentum transfer $q_0 = 0$ [7, 10]. In this work, the parameters U and J_y (see equation (2)) describing the system in the Bose–Hubbard model are almost unaltered by the additional light potential created by the Bragg beams.

The probe we use (Bragg beams) weakly affects the state of the system under investigation and the amount of excitation varies linearly with the parameters of the probe. In this linear response regime, the spectra we measure in the lowest energy band are proportional to the dynamical structure factor S [27].

4. Excitations in inhomogeneous Mott states towards different energy bands

Bragg spectroscopy was used in [20] to investigate the response of inhomogeneous MI states within the lowest energy band and to study their properties on an energy scale of the order of

the Mott gap Δ_{ph} . Excitations to higher energy bands have been recently reported in [47] where the authors focused on the lifetime and the coherence of higher bands population. Here, we study the spectrum of inhomogeneous MI states on a large energy scale, focusing on transitions to high-energy bands of the optical lattice, for a momentum transferred by the Bragg beams $q_{0,y} = 0.96(3)k_L$.

Since the typical energy transferred for excitations in high-energy bands is at least one order of magnitude larger than the Mott gap (see details below), the excited atoms are not correlated to the non-excited ones lying in the lowest energy band. In addition, the Bragg excitation being weak, only a small fraction of the atomic cloud is excited. Therefore, the small amount of atoms excited in the high-energy bands can safely be considered as non-interacting particles. This point makes the study of the high-energy excitation spectrum of a MI state much different from that restricted to the lowest energy band where atom–atom correlations play a crucial role [20].

4.1. Multi-band spectrum of a MI state

As demonstrated for example in [48], the presence of a periodic potential implies the existence of different energy bands in the excitation spectrum, the so-called Bloch bands (see figure 5(a)). The typical tunneling time of atoms in a lattice is $\sim \hbar/J$. When it is smaller than the timescale of the experiment, a 3D BEC loaded in the optical lattice has a long-range phase coherence. Its quasi-momentum distribution in the presence of the optical lattice has a small extension around the center of the first Brillouin zone $q_{i,y} = 0$. Therefore, the resonance in the excitation spectrum is narrow since the resonant condition for a two-photon transition between momentum states $\hbar q_{i,y} = 0$ and $\hbar q_{f,y} = \hbar q_{0,y}$ is well defined in energy. Our experimental resolution is good enough to observe that this spread in energy is a small fraction of the energy bandwidth. As it is shown on figure 5(b), the experimental spectrum of this phase-coherent system ($s_y = 9$, $s_{\perp} = 0$) exhibits several well-defined resonances corresponding to excitations created in the different lattice bands [48].

The case of the array of 1D gases loaded in a 1D optical lattice is different, in particular when the amplitude of the longitudinal lattice is large enough for the 1D gases to be in the MI regime. On the one hand, strong atom–atom correlations are present and are responsible for peculiar features of the Mott state such as the existence of an energy gap Δ_{ph} in the excitation spectrum. On the other hand, the quasi-momentum distribution of a MI is spread over the first Brillouin zone ($-k_L < q_{i,y} < k_L$) as a consequence of the spatial localization of atoms [49]. Deep enough in the Mott regime, this quasi-momentum distribution is expected to be close to homogeneous over the interval $[-k_L; k_L]$. Therefore two-photon transitions towards the excited bands are possible from any initial quasi-momentum and Bragg spectroscopy can create excitations on a large energy interval, of the order of the energy bandwidth of single particle. In this picture, varying the frequency between the Bragg beams allows one to selectively excite (and therefore address) only a fraction of the atomic cloud through the resonance condition: for a given energy transfer lying in the energy interval of an excited band, one can always find a populated quasi-momentum state matching the resonance condition for being excited.

Figure 5(c) depicts a spectrum of 1D gases in the Mott insulating state ($s_{\perp} = 35$, $s_y = 9$). The energy scale is identical to that of a 3D BEC loaded in a 1D optical lattice along the y -axis with the same amplitude $s_y = 9$ (figure 5(b)). On this energy scale, the spectra of 1D MI states exhibit several large resonances that have to be identified with transitions towards different

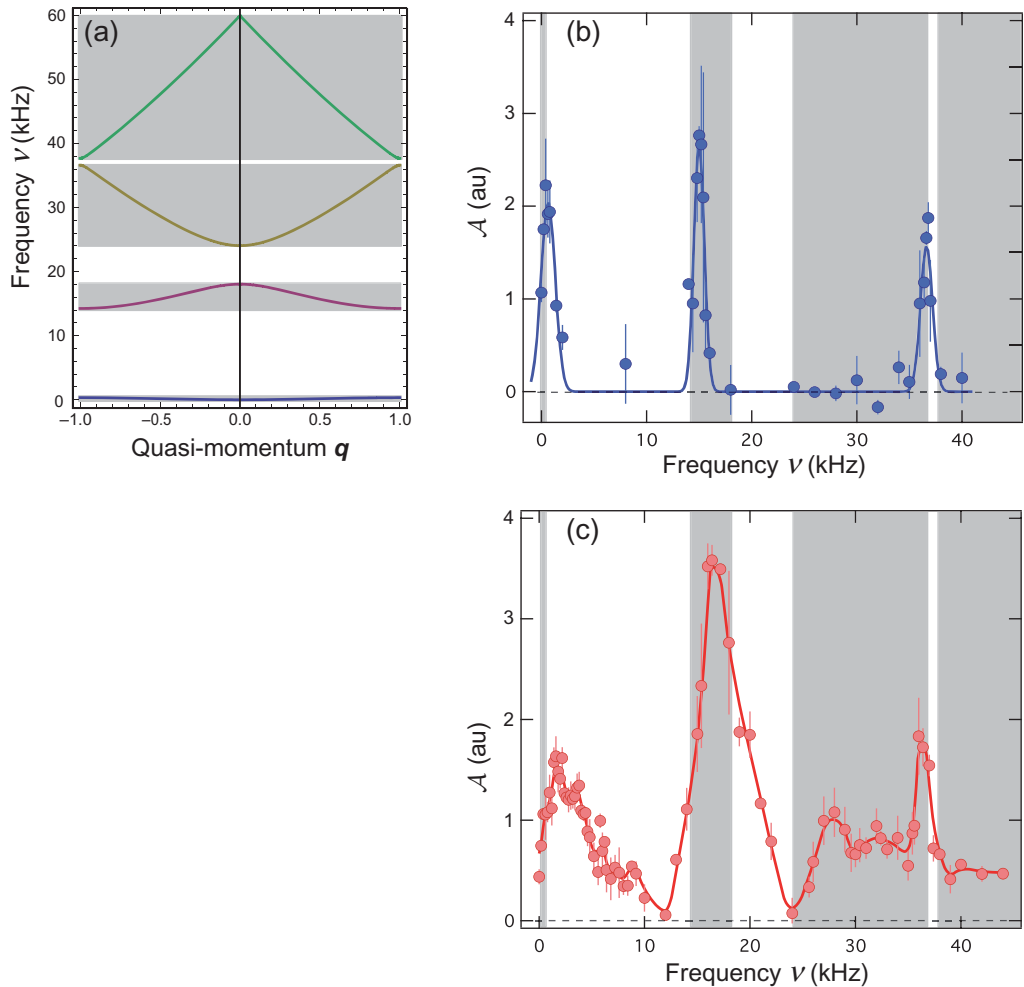


Figure 5. (a) Energy bands of single particles in a periodic potential of amplitude $s = 9$. The gray areas cover the entire energy distribution of each band and they are reported in (b) and (c). (b) Bragg spectrum of a 3D BEC loaded in a 1D optical lattice at the amplitude $s_y = 9$ (blue dots) and for a momentum transfer $\hbar q_{0,y} = 0.96(3)\hbar k_L$. The solid blue line is a fit with three Gaussian functions. (c) Bragg spectra of an array of 1D BECs ($s_{\perp} = 35$) loaded in a 1D optical lattice of amplitude $s_y = 9$ (red dots), i.e. the 1D gases being in the MI state, and for a momentum transfer $\hbar q_{0,y} = 0.96(3)\hbar k_L$. The red solid line is a guide to the eye.

energy bands of the optical lattice. The experimental measurements are reported with single-particle energy bands as gray areas. The lowest energy band ($\nu < 10$ kHz) is much larger than the single-particle energy band due to the presence of atom–atom correlations. A detailed analysis of this effect has been the object of [20]. The energy transfer corresponding to transitions towards high-energy bands is tens of kHz much larger than the Mott gap $\Delta_{\text{ph}} \simeq \hbar \times 2$ kHz [20]. Identifying the final momentum state of atoms giving contribution for the different parts of the excitation spectrum of figure 5(c) should allow us to determine to which band the excitations belong to. To this purpose, we have used a band-mapping technique [46] that we describe in the following paragraph.

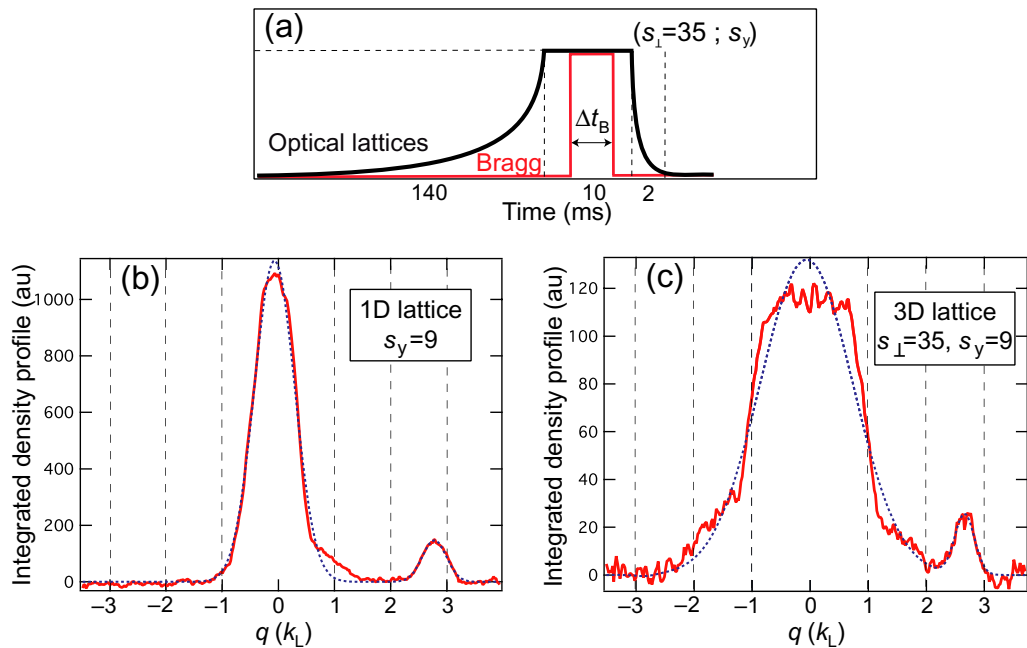


Figure 6. (a) Experimental time sequence of the band-mapping technique. (b) Band population in the case of a 3D BEC in the presence of a 1D optical lattice of amplitude $s_y = 9$ after a Bragg pulse with detuning $\nu = 38$ kHz. (c) Band population in the case of an array of 1D BECs loaded in a 3D optical lattices of amplitudes ($s_{\perp} = 35$, $s_y = 9$) after a Bragg pulse with detuning $\nu = 34$ kHz. The horizontal scale is normalized to the momentum $\hbar k_L$ of the longitudinal optical lattice in both pictures.

4.2. Measurement of the momentum of the excited atoms by the Bragg beams

4.2.1. Band population in a 1D optical lattice. In order to identify the band towards which atoms are excited by the Bragg pulse, we switch off abruptly the magnetic trap and we ramp down the lattice on a timescale (~ 2 ms) too short for interaction-induced thermalization but adiabatic with respect to the atomic motion in a single lattice well [46]. Doing this, one ensures to preserve the band population. After a time-of-flight, the atomic distribution reflects the band population in the momentum space. In practice, we ramp down the optical lattice with an exponential ramp of duration 2 ms and time constant 0.5 ms as sketched in figure 6(a). We first apply this technique to the 3D BEC loaded in a 1D optical lattice with amplitude $s_y = 9$ corresponding to the spectrum of figure 5(b). The density profile along the y -axis after time-of-flight is shown on figure 6(b) when a resonant Bragg pulse creates excitations in the third energy band ($\nu = 38$ kHz). The central peak around $q = 0$ corresponds to the non-excited cloud and it is the only feature left when the Bragg pulse is tuned out of resonance. On resonance a small lateral peak appears corresponding to excited atoms³. The momentum of the excited atoms lies between $2\hbar k_L$ and $3\hbar k_L$, proving that these atoms are excited in the third band of the optical

³ To measure the spectra we excite fewer atoms than the ones which are seen after the band-mapping technique. Indeed, we have changed the parameters of the Bragg beams in the latter case in order to better identify the cloud of the excited atoms.

lattice. Fitting the position of the diffracted cloud with respect to the non-diffracted one with a Gaussian function we have measured momentum transfers of $1.1(1)\hbar k_L$ and $2.8(1)\hbar k_L$ for a Bragg pulse corresponding, respectively, to the transition towards the second and third energy bands of the lattice. These results are in good agreement with the expected values $1.04(3)\hbar k_L$ and $2.96(3)\hbar k_L$ corresponding to a momentum transfer $\hbar q_{0,y} = 0.96(3)\hbar k_L$ given by the Bragg beams in our configuration⁴.

4.2.2. Band population in the Mott insulating states. We turn to the case of the 1D gases in the inhomogeneous MI state ($s_{\perp} = 35, s_y = 9$). The same experimental technique as described above is used to map the band population also in this case. The density profile obtained from the band mapping of the array of 1D gases is shown on figure 6(c). The detuning between the Bragg beams is $\nu = 34$ kHz and corresponds to an excitation that lies in the wide and flat region of the spectrum. As in the case of figure 6(b), the diffracted atoms are clearly visible and lie in the third band of the optical lattice ($2k_L < q < 3k_L$). We note that the central (non-diffracted) peak is larger and flatter over the lowest lattice band with respect to the case of figure 6(b). This observation indicates that the quasi-momentum distribution of the inhomogeneous MI state covers almost uniformly the first band as expected for a system that is not phase coherent.

By applying the same fitting procedure as in the case of figure 6(b), we extract the momentum $\hbar q$ to the diffracted atoms in the case of a 3D lattice with amplitudes ($s_{\perp} = 35, s_y$). We repeat this procedure over the entire frequency range corresponding to the transition towards the third and fourth bands, i.e. varying the relative detuning ν of the Bragg beams from 27 to 45 kHz, with the results plotted in figure 7 for $s_y = 10$. The experimental resolution $\simeq 400$ Hz of the Bragg spectroscopy allows us to do a precise mapping on this large energy scale. In figure 7, we plot the energy transfer $h\nu$ given by the Bragg beams as a function of the momentum of the excited atoms measured using the band-mapping technique. These results are compared with the dispersion relation of single particles in the presence of a periodic potential with an amplitude $s_y = 10$ showing a good agreement⁵. This demonstrates that: (i) the excitations observed over a large energy scale between 27 and 36 kHz (resp between 37 and 45 kHz) correspond to transition towards the third (resp fourth) energy band of the optical lattice; (ii) the quasi-momentum distribution of the inhomogeneous MI state extends over the entire lowest lattice band since the entire energy band can be mapped using a Bragg excitation with a fixed momentum transfer $\hbar q_{0,y}$.

4.3. High-energy bands; towards novel information about the Mott state

Using a band-mapping technique we have demonstrated that the different parts of the spectrum measured in a MI state (see figure 5(c)) can be attributed to the different energy bands induced by the optical lattice. At high energies, e.g. for excitations into the third and the fourth band, the frequency range of the Mott excitations corresponds to the bandwidth of the single-particle spectrum, a feature that is expected since in that situation the typical atom–atom correlation energy Δ_{ph} is much smaller than that of the excited atoms. Yet, as we discuss below, the peculiar

⁴ Note that this technique is not well adapted to the measurement of the momentum transfer for the transition within the lowest energy band since the finite width of the non-diffracted atoms covers a large part of the first band.

⁵ The dispersion relation in the lowest energy band can be considered as flat on the energy scale of figure 7. In figure 7, we have subtracted this constant energy offset to the bare calculation of the single-particle dispersion relation since it does not enter the two-photon transition process.

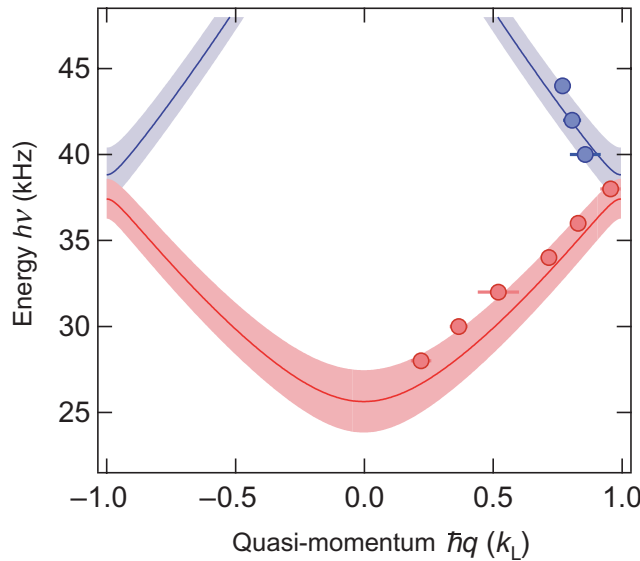


Figure 7. Energy dispersion as a function of the quasi-momentum from the band-mapping technique used after a Bragg pulse. The dots correspond to the experimental measurements and the red and blue colors are associated, respectively, with excitations in the third and fourth bands of the optical lattice. The solid lines are the band dispersion relation for single particles at $s_y = 10$ and the shaded areas correspond to the band dispersion relation taking into account the experimental uncertainty on the calibration of s_y (10%).

lineshape of the response within a given band has to be related to the properties of the many-body state which is probed. Therefore, the identification of the energy scale of a given excited band opens the possibility to study the modulation of the response to the Bragg pulse *within* a single band. For example, the response of the MI state to the Bragg spectroscopy shows a structure in amplitude within the third band (from 25 to 36 kHz) in figure 5(c). In particular, we observe an increased response at both edges of the band. A peak is mostly evident close to the higher energy edge, the position of which corresponds to a Bragg transition from an initial quasi-momentum $q_i = 0$. We now schematically discuss a way to interpret these features.

We expect the atoms excited by the Bragg beams in high-energy bands not to interact with the non-excited ones since their typical energy (corresponding to a frequency of several tens of kHz) is much larger than the particle-hole excitation energy $\Delta_{\text{ph}} \simeq h \times 2$ kHz. In addition, as already mentioned, with our experimental parameters only a minor fraction of the atoms is excited. Therefore, the transition induced by the Bragg beams in high-energy bands can be considered to happen between an initially strongly correlated state (Mott state) and single-particle states: the two-photon transition creates a hole in the Mott state and it populates highly energetic single-particle states. In other words, the response of the gas to the Bragg pulse gives access to the *one-particle spectral function* of the Mott and it implies both the dispersion relation of the hole in the Mott phase and the density of states (DOS) to populate the excited band from the initial correlated phase⁶. Information about the one-particle spectral function of solid-state systems has proved to be crucial to understand properties of correlated states such as high- T_c

⁶ We acknowledge interesting discussions with E Altman and S Huber on this point.

superconductors [50] and recent proposals have demonstrated the interest of measuring the one-particle spectral function for ultracold fermions [51]. We anticipate that the information about the one-particle spectral function obtained from the high-energy bands spectra might shed new light on the bosonic Mott state, in particular close to the SF–MI transition. To our knowledge, no theoretical predictions of such an experimental signal measured with ultracold bosons exist.

The experimental situation is more complex than the case of a homogeneous Mott state. Due to the presence of the longitudinal trap, the 1D gases are in the inhomogeneous MI state formed of Mott regions with different fillings separated by SF areas [17]. This state can be viewed as constituted of domains with narrow quasi-momentum distributions (SF regions) and domains with almost homogeneous quasi-momentum distributions (MI regions), resulting in a nontrivial momentum distribution of the global state. As U/J increases and the system is driven deeper in the Mott phase, the number of atoms which do not belong to a Mott state drops. For this reason, we expect the contribution of the SF domains in the response to the Bragg excitation not to be significant. However, a complete picture taking into account contributions from the different Mott and SF regions has to be developed to interpret the details of the spectrum of figure 5(c). We hope that the measurements presented in this paper could stimulate such theoretical work.

5. Conclusion

In conclusion, we have measured the response of bosonic MI states to excitations induced by inelastic scattering of light. As already demonstrated in [20], this spectroscopic technique is a promising tool to characterize strongly interacting quantum phases. We have presented here in detail the experimental setup and the way the measurement has been carried out. In particular, we have demonstrated that the quantity we measure is proportional to the increase of energy in the gaseous system and that the response to the light scattering is in a perturbative and linear regime.

We have extended our previous work [20] to the study of excitations towards several energy bands in MI states. In contrast to the case of a 3D BEC loaded in a 1D optical lattice, the spectra of these Mott states exhibit broad resonances in energy. The use of a band-mapping technique after applying the Bragg pulse allows us to identify these resonances with transitions towards the different energy bands induced by the optical lattice. We also give direct experimental evidence that the momentum distribution of Mott states spreads over the entire first Brillouin zone. This property enables us to reconstruct the dispersion relation of the high-energy bands using a Bragg excitation at a fixed momentum transfer.

Finally, the amplitude of the response of the inhomogeneous MI state in high-energy bands exhibits peculiar structures within a single excited band. We expect that these could give important information on the experimental system and we think that this point should be the object of future investigation, both experimental and theoretical.

Acknowledgments

We acknowledge E Altman, S Huber and all the colleagues of the Quantum Degenerate Group at LENS for stimulating discussions. This work was supported by UE contract no RII3-CT-2003-506350, MIUR PRIN 2007, Ente Cassa di Risparmio di Firenze, DQS EuroQUAM Project,

NAMEQUAM project and Integrated Project SCALA. This research was supported by a Marie Curie Intra European Fellowship within the 7th European Community Framework Programme (DC).

References

- [1] Dagotto E 1994 *Rev. Mod. Phys.* **66** 763
- [2] Nozieres P and Pines D 1994 *The Theory of Quantum Liquids* (Reading, MA: Addison-Wesley)
- [3] Giamarchi T 2004 *Quantum Physics in One Dimension* (Oxford: Oxford Science Publications)
- [4] Ishii H, Kataura H, Shiozawa H, Yoshioka H, Otsubo H, Takayama Y, Miyahara T, Suzuki S, Achiba Y, Nakatake M, Narimura T, Higashiguchi M, Shimada K, Namatame H and Taniguchi M 2003 *Nature* **426** 540
- [5] Auslaender O M, Yacoby A, de Picciotto R, Baldwin K W, Pfeiffer L N and West K W 2002 *Science* **295** 825
- [6] Schwartz A, Dressel M, Grüner G, Vescoli V, Degiorgi L and Giamarchi T 1998 *Phys. Rev. B* **58** 1261
- [7] Stöferle T, Moritz H, Schori C, Köhl M and Esslinger T 2004 *Phys. Rev. Lett.* **92** 130403
- [8] Spielman I B, Phillips W D and Porto J V 2007 *Phys. Rev. Lett.* **98** 080404
- [9] Greiner M, Mandel O, Esslinger T, Hänsch T W and Bloch I 2002 *Nature* **415** 39
- [10] Fallani L, Lye J E, Guarrera V, Fort C and Inguscio M 2007 *Phys. Rev. Lett.* **98** 130404
- [11] Jördens R, Strohmaier N, Günter K, Moritz H and Esslinger T 2008 *Nature* **455** 204
- [12] Schneider U, Hackermüller L, Will S, Best T, Bloch I, Costi T A, Helmes R W, Rasch W and Rosch A 2008 *Science* **322** 1520
- [13] Fölling S, Gerbier F, Widera A, Mandel O, Gericke T and Bloch I 2005 *Nature* **434** 481
- [14] Guarrera V, Fabbri N, Fallani L, Fort C, van der Stam K M R and Inguscio M 2008 *Phys. Rev. Lett.* **100** 250403
- [15] Lignier H, Zenesini A, Ciampini D, Morsch O, Arimondo E, Montangero S, Pupillo G and Fazio R 2009 *Phys. Rev. A* **79** 041601
- [16] Jaksch D, Bruder C, Cirac J I, Gardiner C W and Zoller P 1998 *Phys. Rev. Lett.* **81** 3108
- [17] Batrouni G G, Rousseau V, Scalettar R T, Rigol M, Muramatsu A, Denteneer P J and Troyer M 2002 *Phys. Rev. Lett.* **89** 117203
- [18] Campbell G K, Mun J, Boyd M, Medley P, Leanhardt A E, Marcassa L G, Pritchard D E and Ketterle W 2006 *Science* **313** 649–52
- [19] Fölling S, Widera A, Müller T, Gerbier F and Bloch I 2006 *Phys. Rev. Lett.* **97** 060403
- [20] Clément D, Fabbri N, Fallani L, Fort C and Inguscio M 2009 *Phys. Rev. Lett.* **102** 155301
- [21] van Oosten D, Dickerscheid D B M, Farid B, van der Straten P and Stoof H T C 2005 *Phys. Rev. A* **71** 021601
- [22] Rey A M, Blakie P B, Pupillo G, Williams C J and Clark C W 2005 *Phys. Rev. A* **72** 023407
- [23] Pupillo G, Rey A M and Batrouni G G 2006 *Phys. Rev. A* **74** 013601
- [24] Kollath C, Iucci A, Giamarchi T, Hofstetter W and Schollwöck U 2006 *Phys. Rev. Lett.* **97** 050402
- [25] Huber S D, Altman E, Büchler H P and Blatter G 2007 *Phys. Rev. B* **75** 085106
- [26] Menotti C and Trivedi T 2008 *Phys. Rev. B* **77** 235120
- [27] Van Hove L 1954 *Phys. Rev.* **95** 249–62
- [28] Ashcroft N W and Mermin N D 1976 *Solid State Physics* (New York: Saunders) p 469
- [29] Kozuma M, Deng L, Hagley E W, Wen J, Lutwak R, Helmerson K, Rolston S L and Phillips W D 1999 *Phys. Rev. Lett.* **82** 871
- [30] Stenger J, Inouye S, Chikkatur A P, Stamper-Kurn D M, Pritchard D E and Ketterle W 1999 *Phys. Rev. Lett.* **82** 4569
- [31] Ozeri R, Katz N, Steinhauer J and Davidson N 2005 *Rev. Mod. Phys.* **77** 187
- [32] Stamper-Kurn D M, Chikkatur A P, Görlitz A, Inouye S, Gupta S, Pritchard D E and Ketterle W 1999 *Phys. Rev. Lett.* **83** 2876
- [33] Steinhauer J, Ozeri R, Katz N and Davidson N 2002 *Phys. Rev. Lett.* **88** 120407

- [34] Steinhauer J, Katz N, Ozeri R, Davidson N, Tozzo C and Dalfovo F 2003 *Phys. Rev. Lett.* **90** 060404
- [35] Richard S, Gerbier F, Thywissen J H, Hugbart M, Bouyer P and Aspect A 2003 *Phys. Rev. Lett.* **91** 010405
- [36] Muniz S R, Naik D S and Raman C 2006 *Phys. Rev. A* **73** 041605
- [37] See for example Müller H, Chiow S, Long Q, Herrmann S and Chu S 2008 *Phys. Rev. Lett.* **100** 180405
- [38] Gerbier F, Thywissen J H, Richard S, Hugbart M, Bouyer P and Aspect A 2004 *Phys. Rev. A* **70** 013607
- [39] Inada Y, Horikoshi M, Nakajima S, Kuwata-Gonokami M, Ueda M and Mukaiyama T 2008 *Phys. Rev. Lett.* **101** 180406
- [40] Papp S B, Pino J M, Wild R J, Ronen S, Wieman C E, Jin D S and Cornell E A 2008 *Phys. Rev. Lett.* **101** 135301
- [41] Veeravalli G, Kuhnle E, Dyke P and Vale C J 2008 *Phys. Rev. Lett.* **101** 250403
- [42] Zambelli F, Pitaevskii L, Stamper-Kurn D M and Stringari S 2000 *Phys. Rev. A* **61** 063608
- [43] Ovchinnikov Yu B, Müller J H, Doery M R, Vredenburg E J D, Helmerson K, Rolston S L and Phillips W D 1999 *Phys. Rev. Lett.* **83** 284
- [44] Menotti C and Stringari S 2002 *Phys. Rev. A* **66** 043610
- [45] Moritz H, Stöferle T, Köhl M and Esslinger T 2003 *Phys. Rev. Lett.* **91** 250402
- [46] Greiner M, Bloch I, Mandel O, Hänsch T W and Esslinger T 2001 *Phys. Rev. Lett.* **87** 160405
- [47] Müller T, Fölling S, Widera A and Bloch I 2007 *Phys. Rev. Lett.* **99** 200405
- [48] Fabbri N, Clément D, Fallani L, Fort C, Modugno M, van der Stam K M R and Inguscio M 2009 *Phys. Rev. A* **79** 043623
- [49] Bloch I, Dalibard J and Zwirger W 2008 *Rev. Mod. Phys.* **80** 885
- [50] Damascelli A, Hussain Z and Shen Z 2003 *Rev. Mod. Phys.* **75** 473
- [51] Dao T, Georges A, Dalibard J, Salomon C and Carusotto I 2007 *Phys. Rev. Lett.* **98** 240402